Inorganic Chemistry

Article

pubs.acs.org/IC

Synthesis, Crystal Structure, and Magnetic Properties of $Li_3Mg_2OsO_6$, a Geometrically Frustrated Osmium(V) Oxide with an Ordered Rock Salt Structure: Comparison with Isostructural $Li_3Mg_2RuO_6$

Phuong-Hieu T. Nguyen,[†] Farshid Ramezanipour,[‡] John E. Greedan,[‡] Lachlan M. D. Cranswick,[§,⊥] and Shahab Derakhshan*[,†]

[†]Department of Chemistry and Biochemistry, California State University, Long Beach, 1250 Bellflower Boulevard, Long Beach, California 90840, United States

[‡]Brockhouse Institute for Materials Research and Chemistry Department, McMaster University, 1280 Main Street West, Hamilton, Ontario, Canada L8S 4M1

[§]Chalk River Laboratory, Canadian Neutron Beam Centre, Chalk River, Ontario, Canada K0J 1J0

Supporting Information

ABSTRACT: The novel osmium-based oxide $Li_3Mg_2OsO_6$ was synthesized in polycrystalline form by reducing Li_5OsO_6 by osmium metal and osmium(IV) oxide in the presence of stoichiometric amounts of magnesium oxide. The crystal structure was refined using powder X-ray diffraction data in the orthorhombic *Fddd* space group with a = 5.88982(5) Å, b = 8.46873(6) Å, and c = 17.6825(2) Å. This compound is isostructural and isoelectronic with the ruthenium-based system $Li_3Mg_2RuO_6$. The magnetic ion sublattice Os^{5+} ($S = {}^3/_2$) consists of chains of interconnected corner- and edge-shared triangles, which brings about the potential for geometric magnetic frustration. The Curie–Weiss law holds over the range 80–300 K with C = 1.42(3) emu·K/mol [μ_{eff} = 3.37(2) μ_B] and θ_C = −105.8(2) K. Below 80 K, there are three anomalies at 75, 30, and 8 K. Those at 75 and 30 K are suggestive of short-range antiferromagnetic correlations, while that at 8 K is a somewhat sharper maximum showing a zero-field-cooled/field-cooled divergence suggestive of perhaps spin freezing. The absence of magnetic Bragg peaks at 3.9 K in the neutron diffraction pattern supports this characterization, as does the absence of a sharp peak in the heat capacity, which instead shows only a very broad maximum at ∼12 K. A frustration index of f = 106/8 = 13 indicates a high degree of frustration. The magnetic properties of the osmium phase differ markedly from those of the isostructural ruthenium material, which shows long-range antiferromagnetic order below 17 K, f = 6, and no unusual features at higher temperatures. Estimates of the magnetic exchange interactions at the level of spin-dimer analysis for both the ruthenium and osmium materials support a more frustrated picture for the latter. Errors in the calculation and assignment of the exchange pathways in the previous report on $Li_3Mg_2RuO_6$ are identified and corrected.

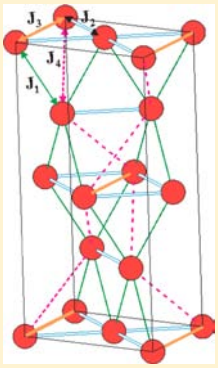

INTRODUCTION

Materials with triangular cationic sublattices with nearest-neighbor antiferromagnetic (AFM) exchange cannot satisfy these spin constraints simultaneously. This phenomenon is known as geometric magnetic frustration (GMF), which results in highly degenerate ground states.[1]

Ordered sodium chloride type transition-metal oxides[2] offer triangular and tetrahedral cationic arrangements and are potential candidates for GMF. There are several known general formulas and structures such as ABO_2, A_2BO_3, A_3BO_4, A_4BO_5, $A_4B_2O_6$, and A_5BO_6,[3−9] where A is a diamagnetic ion and B is a magnetic cation. We are particularly interested in the last composition, which offers various possibilities for GMF. A useful measure of GMF is the frustration index, $f = |\theta|/T_{c,f}$, where θ is the intercept from the Curie–Weiss law and T_c and T_f are the critical temperature for long-range magnetic order and the spin-freezing temperature, respectively.[10]

A_5BO_6 systems crystallize in two symmetries of interest, $C2/m$ and *Fddd*. For $C2/m$ symmetry, we have previously studied two isostructural and isoelectronic, $S = {}^1/_2$, compounds, namely, Li_4MgReO_6[11] and Li_5OsO_6,[12] with drastically different magnetic properties. The rhenium-based compound is highly frustrated with $f \sim 14$ and exhibits spin-glass behavior below 12 K with no long-range order, while the latter undergoes long-range AFM order below 40 K and has a frustration index of ∼1.[12] In *Fddd* symmetry, we reported a novel ruthenate, $Li_3Mg_2RuO_6$,[13] in which Ru^{5+} ($S = {}^3/_2$) ions are arranged in ribbons of edge-sharing triangles that are interconnected by corner sharing to form a three-dimensional geometry (Figure 1, inset). This compound was shown from magnetic susceptibility, heat capacity, and neutron diffraction data to be moderately frustrated with f = 6 and to undergo long-range AFM order below 17 K.[13]

Here we report on the synthesis, crystal structure, and magnetic properties of the isoelectronic and isostructural osmium-based compound $Li_3Mg_2OsO_6$ and compare these properties to those of $Li_3Mg_2RuO_6$. Moreover, to understand

Received: June 22, 2012
Published: October 15, 2012

   dx.doi.org/10.1021/ic3013377 | *Inorg. Chem.* 2012, 51, 11493−11499

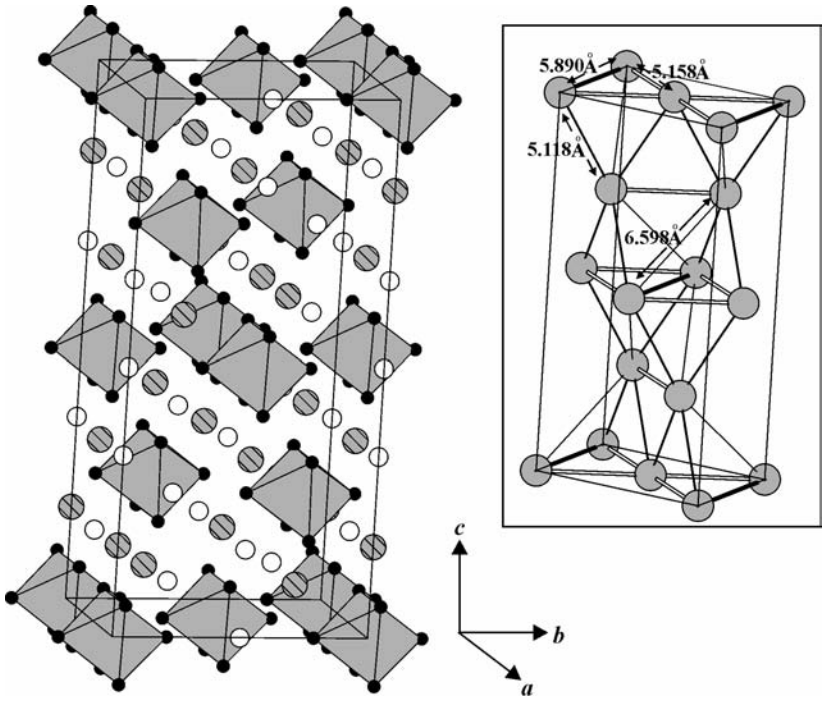

Figure 1. Crystal structure of $Li_3Mg_2OsO_6$. The gray octahedra represent $[OsO_6]^{7-}$, the large gray circles are magnesium-rich positions, and the small empty circles are lithium-rich positions. The inset shows the osmium sublattice.

better the observed magnetic behavior of the new system and also the origin of the observed differences between the two compounds, the calculated relative magnitudes of different spin-exchange interactions are compared.

EXPERIMENTAL SECTION

Synthesis. A stoichiometric mixture of Li_5OsO_6, osmium metal powder (Alfa Aesar, 99.95%), OsO_2 (Alfa Aesar, 99.9%), and MgO (Acros Organics, 99.99%), according to eq 1, was mixed and ground.

$$\frac{3}{5}Li_5OsO_6(s) + 2MgO(s) + \frac{1}{5}OsO_2(s) + \frac{1}{5}Os(s) \Rightarrow Li_3Mg_2OsO_6(s) \quad (1)$$

The powder mixture was then pressed into a pellet, which was placed in an alumina crucible. All of the sample manipulations were performed in an argon-filled glovebox. The crucible was then sealed in an evacuated fused quartz tube. The tube was then placed in a box furnace and was heated at 750 °C for 48 h. The pellet was reground and repressed and the same heating schedule was repeated several times until a homogeneous brown powder was obtained.

Prior to the sample preparation, MgO was heated by a H_2/O_2 flame in a silica tube under dynamic vacuum for 15 min to ensure the removal of trace amounts of moisture and also decomposition of carbonates, which was transferred into the glovebox. The starting material, Li_2O, was prepared by heating lithium hydroxide monohydrate (Alfa Aesar, 98%) to 450 °C in a fused quartz tube under dynamic vacuum for 18 h and was then transferred into the glovebox. To prepare Li_5OsO_6, a mixture of Li_2O and osmium metal powder with a 2.5:1 molar ratio was thoroughly ground and pressed into a pellet in an-argon filled glovebox. The pellet was placed in an alumina boat and heated to 500 °C in a tube furnace under a dynamic argon flow. After 5 h, the argon flow was switched to oxygen, the temperature was raised to 800 °C, and the sample was heated for 12 h and cooled to room temperature in 10 h.[12]

Phase Analyses. To examine the phase purity of the brown $Li_3Mg_2OsO_6$ product, powder X-ray diffraction data were collected, employing a PANalytical X'Pert Pro MPD diffractometer, equipped with a linear X'Celerator detector, with Cu $K\alpha_1$ radiation.

Crystal Structure Determination Using Powder X-ray Diffraction. The crystal structure was determined by Rietveld refinement of the powder X-ray data, using the General Structure Analysis System (GSAS) suite and EXPGUI interface.[14,15] The X-ray diffraction data were collected at room temperature in the range $18° \leq 2\theta \leq 100°$ with ≈0.008° intervals. The structural data from $Li_3Mg_2RuO_6$[13] were used as the initial model for refinement. A pseudo-Voigt peak-shape profile, which is a combination of both Gaussian and Lorentzian functions, was chosen, and the parameters were refined to obtain the best fit to the experimental data. The residual factors are $R_p = 0.0777$ and $wR_p = 0.1092$. The powder X-ray diffraction pattern along with the fit to the structural model is presented in Figure 2.

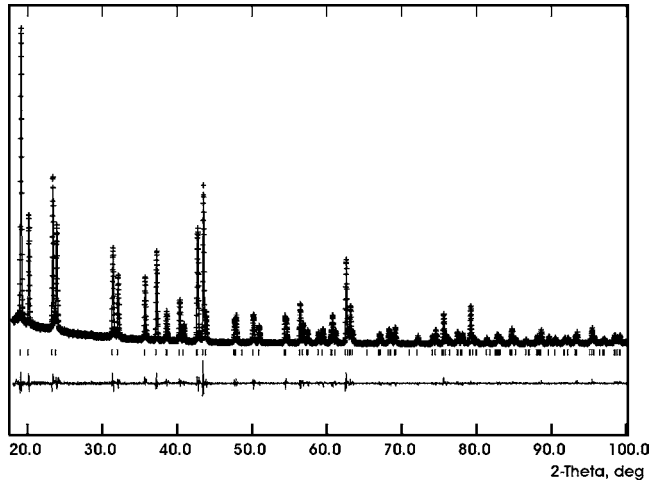

Figure 2. Room temperature powder X-ray diffraction pattern of $Li_3Mg_2OsO_6$. The crosses indicate the experimental data, while the Rietveld refinement fit is shown as a solid line. The bottom thin solid line represents the difference, and the peak positions are located by the vertical tick marks.

dx.doi.org/10.1021/ic3013377 | Inorg. Chem. 2012, 51, 11493−11499

Neutron Powder Diffraction. Neutron powder diffraction data were collected using the C2 diffractometer at the Canadian Neutron Beam Centre with wavelengths λ = 1.3303 and 2.3715 Å at 300 and 3.8 K.

Magnetic Susceptibility Measurement. A polycrystalline powder sample of $Li_3Mg_2OsO_6$ was encased in a gelatin capsule, and magnetic susceptibility data were collected by employing a Quantum Design MPMS SQUID magnetometer. Both zero-field-cooled (ZFC) and field-cooled (FC) data were obtained over the temperature range of 5−300 K at an applied field of 1000 Oe. Magnetization versus field measurements, up to 5.5 T, were performed at 2 and 300 K.

Heat Capacity Measurements. Heat capacity data were collected from 3.2 to 30 K by employing the heat capacity probe of the Oxford MagLab system. The powder sample was pressed into a thin pellet, and a small piece, 3.47 mg, was mounted onto a sapphire measurement chip with Apeizon grease. Contributions of the grease and sample holder chip to the measured heat capacity were subtracted. Data were collected at 0 and 9 T.

Theoretical Calculations and Spin-Dimer Analyses. The relative values of the various spin-exchange pathways were estimated by performing extended Hückel spin-dimer analyses.[16] The magnetically active centers, OsO_6^{7-} units, interact with each other by only supersuperexchange (SSE) mechanisms. For each pathway that involves two discrete OsO_6^{7-} octahedra ($Os_2O_{12}^{14-}$ dimer), the intersite hopping energy, Δe, was estimated using the *CAESAR* package.[17] For the O s and p and Ru d states, double-ζ Slater-type orbitals (STOs) were employed, whereas single-ζ STOs were chosen for the Os s and p states. The values of the ζ_i and ζ'_i coefficients and valence-shell ionization potentials H_{ii} used for the calculations are presented in Table 1. The hopping energy for each exchange pathway

Table 1. Values for the ζ_i Coefficients and Valence-Shell Ionization Potentials H_{ii} of the Atomic STOs Employed for the Spin-Dimer Calculations for $Li_3Mg_2OsO_6$

atom	orbital	H_{ii} (eV)	ζ_i	C	ζ'_i	C'
O	2s	−32.300	2.688	0.7076	1.675	0.3745
O	2p	−14.8000	3.694	0.3322	1.659	0.7448
Os	6s	−8.1700	2.400	1		
Os	6p	−4.810	1.770	1		
Os	5d	−11.840	4.504	0.6066	2.391	0.5486

is related to the magnetic exchange interaction by $J \cong \langle(\Delta e)^2\rangle/U$. Because the Coulomb forces, U values, are identical for all of these interactions, one can estimate the relative magnitudes of the various J's, knowing the $\langle(\Delta e)^2\rangle$ values.

RESULTS AND DISCUSSION

Crystal Structure. $Li_3Mg_2OsO_6$ crystallizes in the orthorhombic *Fddd* space group in an ordered rock salt structure type with lattice dimensions a = 5.88982(5) Å, b = 8.46873(6) Å, and c = 17.6825(2) Å. The structure is composed of edge-shared octahedra with eight formula units per unit cell (Figure 1). There are four independent cationic positions in the unit cell. Os^{5+} has a significantly different formal charge and ionic radius from Li^+ and Mg^{2+}. The ionic radii for the three cations are Li^+ = 0.76 Å, Mg^{2+} = 0.72 Å, and Os^{5+} = 0.565 Å,[18] which drives Os^{5+} to reside in a separate crystallographic position. However, the other three cationic sites are mixed occupied by lithium and magnesium with different fractions. M1 was determined to be a magnesium-rich site, while M2 and M3 are lithium-rich sites. The chemical composition was refined to $Li_{2.73(1)}Mg_{2.27}OsO_6$; however, the inherent limitations of powder X-ray diffraction when dealing with light elements such as lithium should be noted. For example, attempts to refine simultaneously the thermal displacement parameters and site occupation ratios for these positions resulted in divergence. Accordingly, the displacement parameters were fixed at arbitrary but reasonable values of 0.01 for M1 and 0.015 for M2 and M3, and the occupation rates were refined. Thus, the occupancy refinements are not quantitatively reliable but can provide semiquantitative measures of the lithium/magnesium site preferences. The unit cell parameters and the refinement parameters are summarized in Tables 2 and 3, respectively. Note that coordination of both Os^{5+} and Ru^{5+} (Table 4) in these isostructural phases is that of an essentially perfect octahedron within error.

Table 2. Unit Cell Constants of Orthorhombic, *Fddd*, $Li_3Mg_2RuO_6$ and $Li_3Mg_2OsO_6$

	a (Å)	b (Å)	c (Å)	V (Å^3)
Li_3MgRuO_6	5.8759(2)	8.4206(1)	17.6455(5)	873.07
Li_3MgOsO_6	5.88981(5)	8.46877(6)	17.6824(2)	881.99

Magnetic Susceptibilities. Inverse susceptibility data from 2 to 300 K are shown in Figure 3a. The data from 100 to 300 K fit well (R^2 = 0.9998) to the Curie−Weiss law, $\chi = C/(T - \theta)$. The derived parameters are C = 1.42(3) emu·K/mol and θ = −105.8(2) K. The effective magnetic moment, μ_{eff}, calculated from the Curie constant is 3.37(2) μ_B, which is lower than the spin-only value for a 5d^3, $S = {}^3/_2$ ion, 3.873 μ_B. Note that, for a nd^3 configuration in nominally octahedral symmetry, the orbital angular momentum L = 0 in the ground electronic state. Orbital contributions can be mixed into the ground state by spin−orbit coupling to the empty excited states, and for less than half-filling, these subtract from the spin component. The observed μ_{eff} is smaller than that previously found for $Li_3Mg_2RuO_6$, 3.60(2) μ_B, which is due to the larger spin−orbit coupling effect in 5d ions compared with 4d ions. The observed Weiss temperature, θ, is nearly the same as that for the ruthenium phase, −109 K.

Figure 3b shows the ZFC and FC susceptibility below the Curie−Weiss regime for $Li_3Mg_2OsO_6$. Data for the corresponding ruthenium phase over the same range are also shown. There are three main features in the data for the osmium compound. First, there is a broad maximum around 70 K, which is likely indicative of short-range AFM spin correlations. A comparable feature is not prominent in the corresponding data for $Li_3Mg_2RuO_6$.[13] There is another broad feature, less obvious, near 30 K, also absent in the ruthenium phase data. Finally, there is an apparently sharper maximum near 8 K that is accompanied by a ZFC/FC divergence. Note that the maximum for the ruthenium phase occurs at 17 K, and there is no ZFC/FC divergence. Such significant differences between two isostructural and isospin materials are unexpected. Taking the 8 K feature for the osmium compound as a phase transition of an as-yet-undetermined type, the frustration index for $Li_3Mg_2OsO_6$ is $f \sim 13$, twice the value for $Li_3Mg_2RuO_6$, indicating that the former is significantly more frustrated than the latter. In Table 5, the magnetic properties of $Li_3Mg_2OsO_6$ are compared with those of $Li_3Mg_2RuO_6$. Figure 3c shows the dependence of the magnetic moment on the applied field at 2 and 300 K for $Li_3Mg_2OsO_6$. Note the linear behavior at 300 K, consistent with paramagnetism and the weak hysteresis at 2 K, which is expected because of the ZFC/FC divergence below 8 K. Interestingly, there the curve is slightly concave, which is not inconsistent with an AFM-type ground state.

dx.doi.org/10.1021/ic3013377 | *Inorg. Chem.* 2012, 51, 11493−11499

Table 3. Atomic Coordinates, Occupancy Factors, and Equivalent Isotropic Displacement Parameters for $Li_3Mg_2OsO_6$ Refined in *Fddd*

	x	*y*	*z*	Li/Mg occ.	U_{iso} (Å^2)
Os	0.125	0.125	0.125		0.0065(2)
M1	0.125	0.125	0.2943(2)	0.26(1)/0.74	0.01
M2	0.125	0.625	0.2892(5)	0.76(1)/0.24	0.015
M3	0.125	0.625	0.125	0.69(1)/0.31	0.015
O1	0.125	0.3629(6)	0.125		0.009(1)
O2	0.1110(6)	0.3743(4)	0.2921(3)		0.011(1)

Table 4. Coordination Sphere of M^{5+} in $Li_3Mg_2MO_6$ (M = Ru and Os) Refined in *Fddd*

	Os	Ru
2 × M−O1 (Å)	2.014(5)	1.958(3)
4 × M−O2 (Å)	2.020(4)	1.966(3)

Table 5. Comparison of the Magnetic Properties of $Li_3Mg_2OsO_6$ with Those of $Li_3Mg_2RuO_6$

	T_N (K)	θ (K)	μ_{eff} (μ_B)	*f*
$Li_3Mg_2RuO_6$	18	−108.7(5)	3.60(2)	6
$Li_3Mg_2OsO_6$	8	−105.8(2)	3.37(2)	13

Heat Capacity. Heat capacity data for $Li_3Mg_2OsO_6$ are shown in Figure 4 for both 0 T (solid circles) and 9 T (open circles) applied field along with those for the potential lattice match compound $Li_3Mg_2NbO_6$ (open triangles). Note the absence of any sharp λ-shaped anomaly near 8 K, the susceptibility maximum, and indeed the maximum in the heat

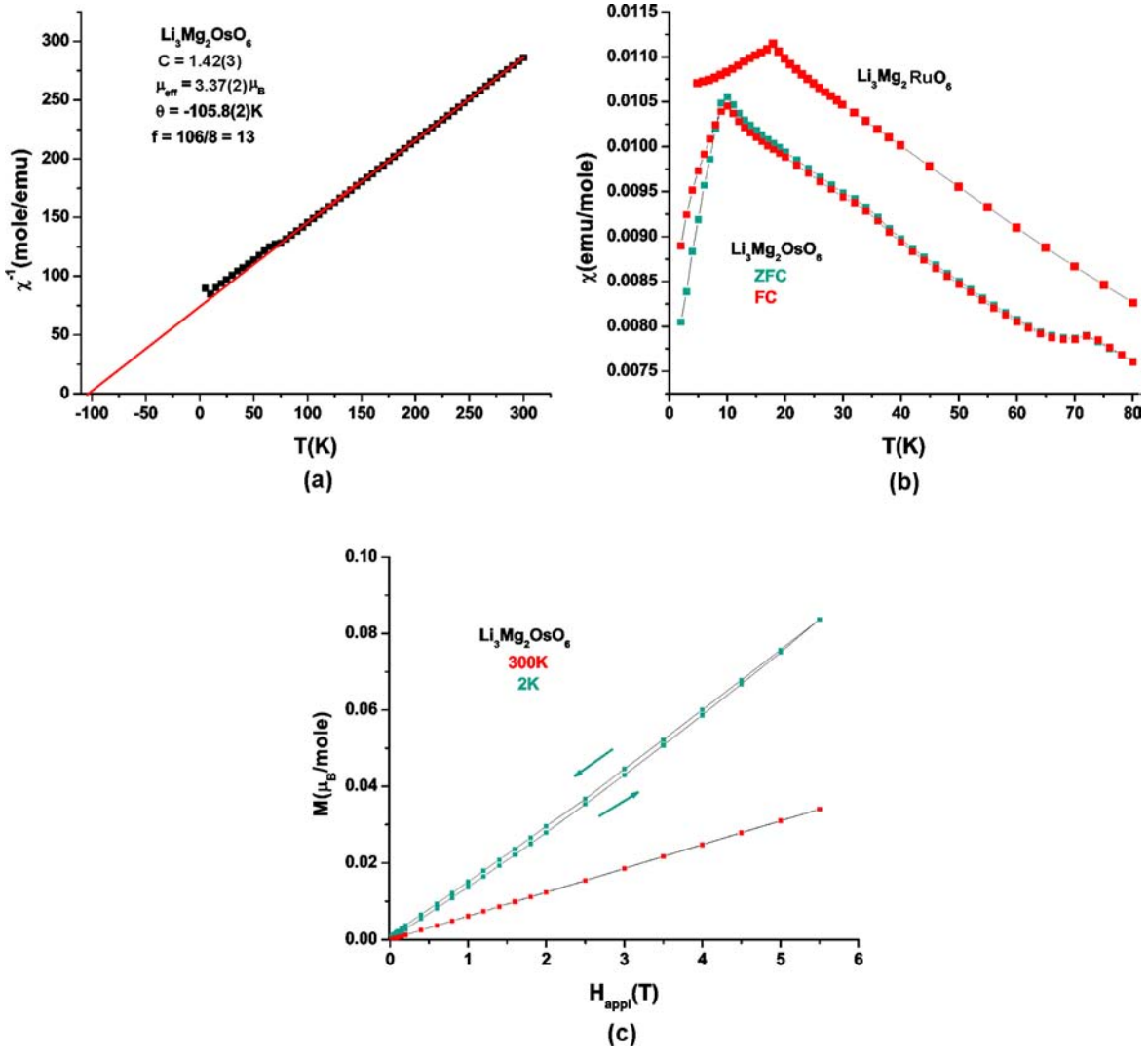

Figure 3. (a) Curie−Weiss fit in the paramagnetic region, 100−300 K. The black squares denote the inverse susceptibility values, and the red line represents the fit. The fitting parameters are shown on the figure and discussed in the text. (b) Temperature-dependent ZFC/FC magnetic susceptibility data for $Li_3Mg_2OsO_6$ between 2 and 80 K compared with ZFC data for $Li_3Mg_2RuO_6$. (c) Field dependence of the magnetic moment for $Li_3Mg_2OsO_6$ at 2 and 300 K.

dx.doi.org/10.1021/ic3013377 | *Inorg. Chem.* 2012, 51, 11493−11499

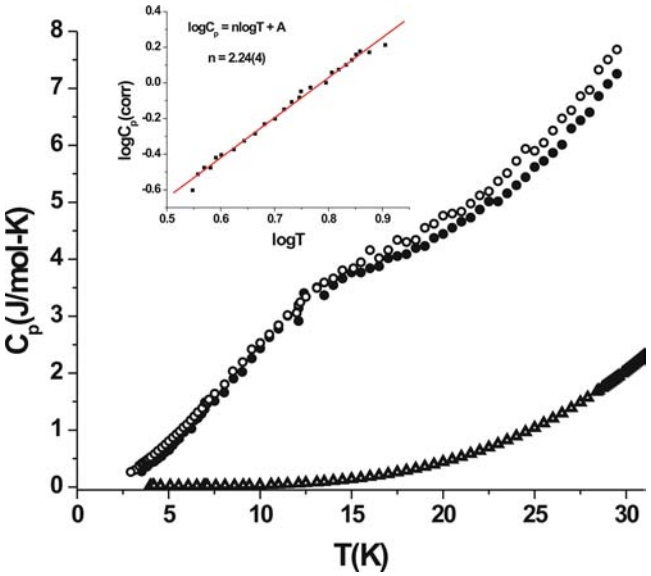

Figure 4. Heat capacity data for $Li_3Mg_2OsO_6$ at 0 T (solid circles) and 9 T (open circles). Data for the potential lattice match material, $Li_3Mg_2NbO_6$, are shown as triangles. The inset shows a fit to the power law $C_p(\text{mag}) = AT^n$ applied to the 0 T data after subtraction of the lattice component.

capacity data appears to lie near ~12 K. This observation rules out long-range magnetic order. There is a minimal effect of the magnetic field. In addition, shown in the inset, the low-temperature heat capacity, corrected for the lattice component, follows the power law $C_p = AT^n$, with $n \sim 2$ over the range 3.2–8.1 K. The exponent is also unchanged in the 9 T field. These results are not typical of canonical spin glasses for which $n = 1$ as has been reported for $Y_2Mo_2O_7$, for example, but are reminiscent of the frustrated but apparently disorder-free spin glass Sr_2CaReO_6, where the unusual exponent $n = 3$ was found along with a robustness with respect to large applied fields.[19,20]

Neutron Diffraction. Neutron diffraction data were collected on a ~3 g sample containing a second monoclinic phase of estimated composition $Li_{3+x}Mg_{2-x}OsO_6$ at the ~5% level and a trace amount of unreacted MgO (Figure 5). The monoclinic phase appears to be isostructural with Li_4MgReO_6, $C2/m$, suggesting that it is an oxidized version of $Li_3Mg_2OsO_6$, but the low concentration renders a definitive characterization difficult. Thus, a multiphase refinement was not carried out. This sample did exhibit the 8 K magnetic transition in the susceptibility data. Neutron data were collected at 3.8 and 300 K to search for evidence of magnetic Bragg peaks. Note that the sample used for the bulk susceptibility and heat capacity measurements was single phase.

Note the absence of magnetic Bragg peaks for the osmium-based material. This is further evidence for the short-range nature of the magnetic correlations exhibited by this compound below 80 K. More detailed neutron diffraction studies with considerably enhanced signal-to-noise quality will be needed to characterize the short-range magnetic correlations.

Computational Analysis: Spin-Dimer Calculations. The Os^{5+} sublattice is shown in Figure 6, along with all of the nearest-neighbor magnetic exchange pathways. If the relative magnitudes of the pathways along the sides of the triangles are comparable, the condition for geometric frustration is present. All of the interactions are of the SSE type; the four most important of these out to an Os–Os distance of 6.598 Å are

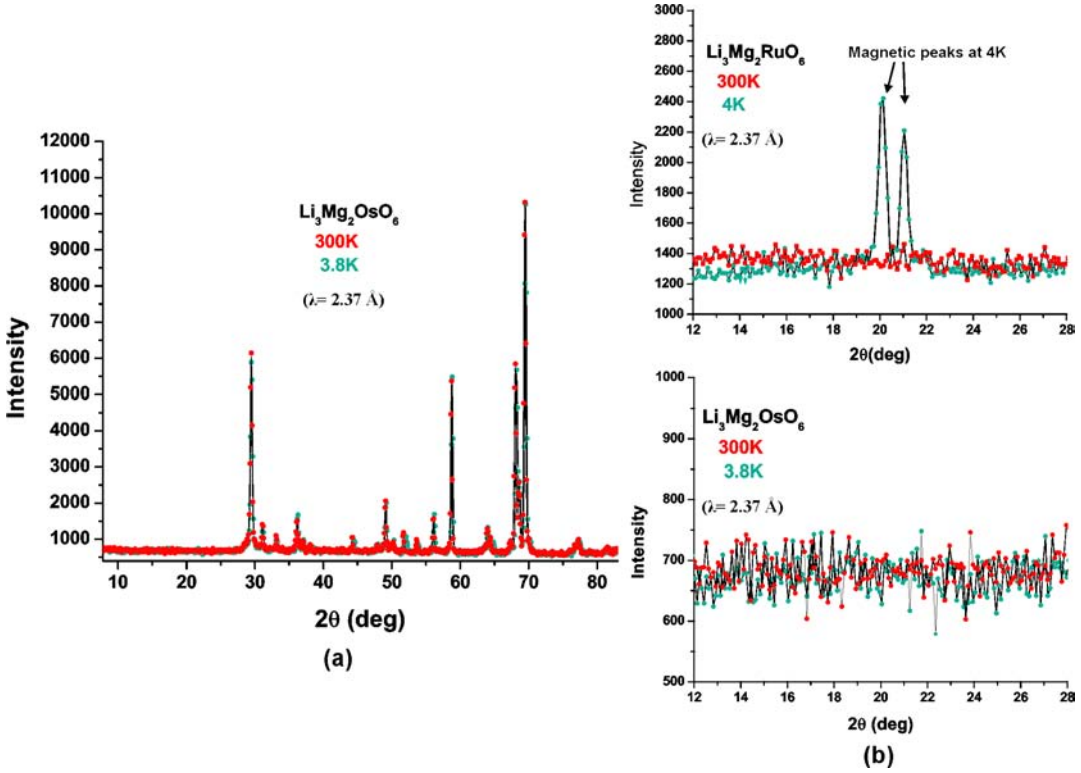

Figure 5. (a) Comparison of the neutron diffraction patterns of $Li_3Mg_2OsO_6$ at 300 K (red circles) and 3.8 K (blue circles). (b) Low-angle data for both $Li_3Mg_2RuO_6$ (top) and $Li_3Mg_2OsO_6$ (bottom) showing the presence of Bragg magnetic peaks for the ruthenium phase and their absence for the osmium material.

dx.doi.org/10.1021/ic3013377 | Inorg. Chem. 2012, 51, 11493–11499

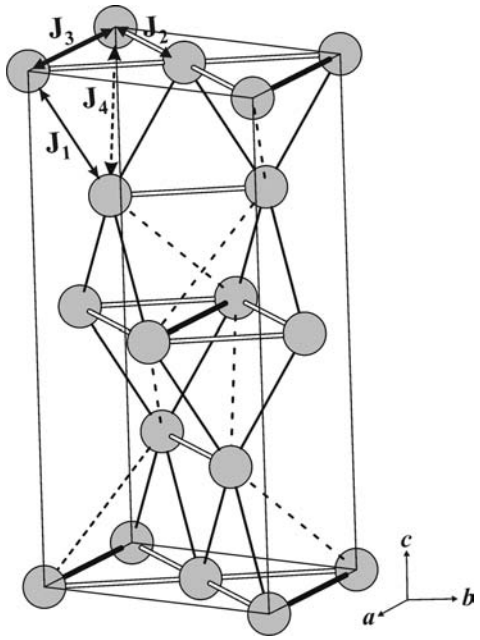

Figure 6. Schematic representation of all nearest-neighbor Os−Os exchange pathways. The gray circles denote Os^{5+} ions. J_1 is represented by the thin lines, J_2 and J_3 are shown by the white and black thick lines, respectively, and J_4 is indicated by the dashed lines.

shown in Table 6. The distances for various interactions are compared with those in $Li_3Mg_2RuO_6$.

Table 6. Relevant Distances to the Four Identified Exchange Pathways, J_1, J_2, J_3, and J_4

	J_1 distance (Å)	J_2 distance (Å)	J_3 distance (Å)	J_4 distance (Å)
M = Ru	5.105	5.135	5.877	6.583
M = Os	5.118	5.158	5.890	6.598

Os^{5+} in an octahedral crystal field with $5d^3$ electronic contribution is an orbital singlet, and no Jahn−Teller distortion is expected, so it is a valid approximation that all t_{2g} orbitals contribute equally to the exchange interactions, and we have

$$\left\langle (\Delta e)^2 \right\rangle \approx \frac{1}{N^2} \sum_{\mu=1}^{N} (\Delta e_{\mu\mu})^2 \tag{2}$$

In these systems, there are three states that are involved, and therefore eq 2 can be rearranged as

$$\left\langle (\Delta e)^2 \right\rangle \approx \frac{1}{9}[(\Delta e_{11})^2 + (\Delta e_{22})^2 + (\Delta e_{33})^2] \tag{3}$$

and finally the spin-exchange interaction constants will be given by

$$J \cong \frac{\langle (\Delta e)^2 \rangle}{U} \tag{4}$$

The relative exchange interactions were calculated, and the results are compared with those of the ruthenium-based compound in Table 7. Note that the values for the ruthenium phase and the figure identifying the exchange pathways differ from those reported previously.[13] This is due to an error in the earlier work that has been corrected here.

Table 7. Relative *J* Values for the Various Exchange Pathways in $Li_3Mg_2MO_6$ (M = Ru and Os) Calculated on the Spin-Dimer Model

pathway	M = Ru, relative	M = Os, relative
J_1	1	0.71
J_2	0.92	1
J_3	0.30	0.86
J_4	0.03	0.08

For both compounds, J_4 is smaller by 1 order of magnitude and can be neglected. J_1, J_2, and J_3 are the dominant interactions, which result in two types of triangles. One set appears as an array of both edge- and corner-sharing triangles in the *ab* plane, formed by J_2 and J_3 type interactions, resembling a two-dimensional network. The other set is composed of J_1 and J_2 type interactions. These corner-shared triangular units connect the former set along the *c* axis and result in a three-dimensional magnetic lattice.

In the osmium-based compound, J_1, J_2, and J_3 are of comparable strength, which is consistent with the condition for GMF. In the ruthenium material, J_3 is smaller by about a factor of 3 than the other two, which is a less ideal situation for full GMF. This analysis provides a possible basis for understanding the larger frustration index for the osmium-based compound and perhaps the apparent lack of true long-range magnetic order.

CONCLUSION

The novel osmium-based compound $Li_3Mg_2OsO_6$ was successfully synthesized. The crystal structure was refined by the Rietveld method from powder X-ray data based on the structural model of isostructural ruthenium-based compound $Li_3Mg_2RuO_6$. Temperature-dependent magnetic susceptibility data revealed that $Li_3Mg_2OsO_6$ exhibits significantly different magnetic behavior, showing three broad maxima in the direct-current susceptibility at 8, 30, and 70 K than $Li_3Mg_2RuO_6$, which has a single sharper feature at 17 K, known to be due to long-range AFM order. While the apparent transition at ∼70 K might be intrinsic, its presence due to an impurity phase cannot be ruled out. Both heat capacity and neutron diffraction data indicate that a long-range-ordered ground state is not attained in $Li_3Mg_2OsO_6$ above 2 K. The nature of the ground state is unclear because the low-temperature heat capacity exhibits a power law exponent $n = 2$ rather than $n = 1$ found for canonical spin glasses. We cannot rule out conclusively the possibility that the absence of a sharp λ anomaly in the heat capacity data is due to poor thermal coupling in the pressed powder sample, but we note that the absence of magnetic reflections in the neutron data supports the conclusion that long-range magnetic order does not occur in this material in the investigated temperature range. In addition, the frustration index for the osmium-based material is 13, more than twice the value for the ruthenium analogue. Spin-dimer analysis, employing extended Hückel theory, suggests that this is due to the equivalence of the three key nearest-neighbor exchange interactions for the osmium-based compound, which provides a more ideal situation for full GMF. Without further evidence on the nature of the magnetic ground state, it is not possible to evaluate the role of the observed lithium/magnesium site disorder. One can only observe that the same level of disorder is present in $Li_3Mg_2RuO_6$ and, in this case, was not sufficient to destroy long-range AFM order.

dx.doi.org/10.1021/ic3013377 | *Inorg. Chem.* 2012, 51, 11493−11499

■ ASSOCIATED CONTENT

Supporting Information

X-ray crystallographic file in CIF format. This material is available free of charge via the Internet at http://pubs.acs.org.

■ AUTHOR INFORMATION

Corresponding Author

*E-mail: shahab.derakhshan@csulb.edu.

Notes

The authors declare no competing financial interest.

[⊥]Deceased.

■ ACKNOWLEDGMENTS

We thank Paul Dube for his assistance in collecting magnetic susceptibility and heat capacity data. S.D. acknowledges support from the Research Corporation for Science Advancement via the Cottrell College Award 19761 and from the DoD Research and Educational Program for HBCU/MI. J.E.G. acknowledges the Natural Sciences and Engineering Research Council of Canada for financial support of this work. The Canadian Neutron Beam Center is funded jointly by NSERC and National Research Council of Canada.

■ REFERENCES

(1) Greedan, J. E. *J. Mater. Chem.* **2001**, *11*, 37.
(2) Mather, G. C.; Dussarat, C.; Etorneau, J.; West, A. R. *J. Mater. Chem.* **2000**, *10*, 2219.
(3) Delmas, C.; LeFlem, G.; Fouassier, C.; Hagenmuller, P. *J. Phys. Chem. Solids* **1978**, *39*, 55.
(4) Soubeyroux, J. L.; Fruchart, D.; Delmas, C.; LeFlem, G. *J. Magn. Magn. Mater.* **1979**, *14*, 159.
(5) Hirota, K.; Nakazawa, Y.; Ishikawa, M. *J. Phys.: Condens. Matter* **1991**, *3*, 4721.
(6) Reimers, J. N.; Dahn, J. R.; Greedan, J. E.; Stager, C. V.; Liu, G.; Davidson, I.; Vonsachen, U. *J. Solid State Chem.* **1991**, *102*, 542.
(7) Clarke, S. J.; Fowkes, A. J.; Harrison, A.; Ibberson, R. M.; Rossiensky, M. J. *Chem. Mater.* **1998**, *10*, 372.
(8) Greedan, J. E.; Raju, N. P.; Davidson, I. J. *J. Solid State Chem.* **1997**, *28*, 209.
(9) Wills, A. S.; Raju, N. P.; Morin, C.; Greedan, J. E. *Chem. Mater.* **1999**, *11*, 1936.
(10) Schiffer, P.; Ramirez, A. P. *Comments Condens. Matter Phys.* **1996**, *18*, 21.
(11) Bieringer, M.; Greedan, J. E.; Luke, G. *Phys. Rev. B* **2000**, *62*, 6521.
(12) Derakhshan, S.; Greedan, J. E.; Cranswick, L. M. D. *Phys. Rev. B* **2008**, *77*, 14408/1.
(13) Derakhshan, S.; Greedan, J. E.; Katsumata, T.; Cranswick, L. M. D. *Chem. Mater.* **2008**, *20*, 5714.
(14) Larson, A. C.; Von Dreele, R. B *General Structure Analysis System (GSAS)*; Los Alamos National Laboratory Report LAUR; Los Alamos National Laboratory : Los Alamos, NM, 2000; p 86.
(15) Toby, B. H. *J. Appl. Crystallogr.* **2001**, *34*, 210.
(16) Whangbo, M. H.; Koo, H. J.; Dai, D. J. *J. Solid State Chem.* **2003**, *176*, 417.
(17) Ren, J.; Liang, W.; Whangbo, M. H. Crystal and Electronic Structure Analysis Using CAESAR. http://www.primeC.com, 2005.
(18) Shannon, R. D. *Acta Crystallogr., Sect. A* **1976**, *32*, 751.
(19) Raju, N. P.; Gmelin, E.; Kremer, R. *Phys. Rev. B* **1992**, *46*, 5405.
(20) Wiebe, C. R.; Greedan, J. E.; Luke, G. M.; Gardner, J. S. *Phys. Rev. B* **2002**, *65*, 144413.